

Dual toroidal photoelectron spectrometer for investigating photodouble ionization in atoms and molecules

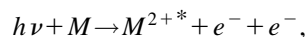
T. J. Reddish, G. Richmond, G. W. Bagley, J. P. Wightman, and S. Cvejanović^{a)}
Physics Department, The University, Newcastle-upon-Tyne, NE1 7RU, United Kingdom

(Received 2 January 1997; accepted for publication 16 April 1997)

A photoelectron-photoelectron coincidence spectrometer, incorporating two independent toroidal analyzers, has been developed to study photodouble ionization of gas targets using synchrotron radiation. The energy-resolved and angle-dispersed electron images are recorded using two-dimensional position-sensitive detectors. The design and performance of the spectrometer is described, with particular emphasis on the electron optical properties of toroidal deflectors and their associated electrostatic lenses. The operation and calibration of the spectrometer are discussed and sample ($\gamma, 2e$) results of helium are presented. © 1997 American Institute of Physics. [S0034-6748(97)02407-6]

I. INTRODUCTION

An exciting new development in photoionization experiments has occurred during the last decade in the area of photodouble ionization (PDI), i.e.,



where * denotes the possibility of the doubly ionized atom or molecule being in an excited state. This field has blossomed because of larger vacuum ultraviolet (vuv) light intensities at synchrotron radiation sources and due to the development of efficient coincidence techniques necessary for the detection of the photoionization fragments. A variety of methods have been employed,¹⁻⁶ depending on which two of the three products are detected. The information obtained is generally complementary but each method provides its own unique insight into the process. PDI is of fundamental interest and importance as double ionization is a multielectron process, depending strongly on electron correlation and so cannot be described by the familiar independent electron model of the atom. Atomic PDI results in an ion and two escaping electrons which are subject to long-range Coulomb forces. A sensitive and direct way of studying the classic three-body Coulomb continuum problem is to use synchrotron radiation and measure the angular distributions of the two outgoing electrons. Such measurements^{1,2,7-10} have only become feasible during the last few years and have provided a powerful stimulus for detailed theoretical investigations.¹¹⁻¹⁴ PDI of helium is the archetypal system for these studies. This is because a bare nucleus is left behind and because no process other than direct double ionization can occur. In contrast, all heavier atoms are subject to other (indirect) processes involving intermediate configurations (i.e., ionic and neutral states converging to higher double ionization thresholds) which also lead to the production of doubly charged ions.

We have developed a spectrometer based on a toroidal geometry, which has properties ideally suited for measuring the angle distributions of the escaping slow (1–50 eV) electrons. Toroidal analyzers have the capability to energy select

the photoelectrons while *preserving* the initial angle of emission. As a direct consequence of their focusing properties,¹⁵ the angular distribution of the electrons is mapped directly onto the detector. Although toroidal analyzers are being developed in a variety of fields,^{7,16-20} their design and operation is not well established nor trivial. Our dual toroidal configuration is unique for PDI experiments and we have also developed complex multielement electron lenses, based on cylindrical and conical geometries, which could be applied to other types of electron spectrometers. Consequently, this article presents our novel electron optical system and a rationale for its design, along with a description of the normalization procedure to correct for inevitable variations in the analyzer's angular efficiency.

II. THE TOROIDAL SPECTROMETER

The apparatus is a photoelectron-photoelectron multicoincidence spectrometer in which the two electrons, of specified energies, are detected over a wide range of emission angles. It has been designed to operate at the Daresbury Synchrotron Radiation Source (SRS) and currently uses vuv radiation from beamline 3.3. The spectrometer is housed in a cylindrical stainless-steel chamber, lined internally with two coaxial mumetal cylinders and evacuated by two Leybold 1000 l/s turbomolecular pumps. A schematic diagram of the apparatus is shown in Fig. 1, indicating the relative orientation of the two partial toroidal analyzers and their respective detectors. The electrostatic analyzers are independent, i.e., they are able to detect dissimilar electron energies, with different resolutions. Electrons emerge from the central interaction region defined by the intersection of the photon and gas beams. Photoelectrons emitted in the plane orthogonal to the photon beam that enter the analyzers are focused at the toroidal entrance slit. Electrons of a specific energy traverse the gap between two toroidal surfaces to the exit slits of each analyzer. The exit lenses accelerate and refocus the energy-resolved electrons to their respective two-dimensional position-sensitive detectors. The final images are circular arcs in shape (with circle centers on the photon axis), in which the position around the perimeter is directly related to the initial azimuthal photoelectron emission angle.

^{a)}Permanent address: Institute of Physics, University of Belgrade, P.O. Box 57, 11001 Belgrade, Yugoslavia.

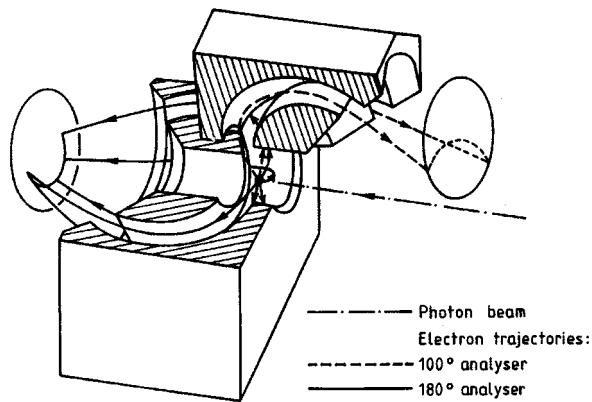


FIG. 1. A schematic diagram showing the configuration of the two partial toroids along with lines indicating central trajectories of electrons with a selection of emission angles, as discussed in the text. The electron lenses are not shown for reasons of clarity. The mechanical angular acceptances of the two analyzers in the plane orthogonal to the photon beam are 100° and 180° .

The multicoincidence capability can be realized as electrons arriving anywhere on one detector can be correlated with electrons detected simultaneously anywhere on the other detector. This enables independent angular distributions [or triple differential cross sections (TDCS)] to be measured *concurrently*. This capability is one of the novel features of the apparatus and is a great asset in compensating for the small ($\gamma, 2e$) cross sections. Furthermore, by rotation of the whole spectrometer around the linearly polarized light source, an arbitrary choice of the emission angle of one electron can be made.

The photoelectron spectrometer is also capable of functioning effectively in a “threshold” mode in which one extracts low energy (0–10 meV) electrons over 4π steradians by the field-penetration technique.²¹ Although the angular resolving capability of toroidal analyzers is superfluous for this type spectroscopy, the possibility to further select the detector’s area which comprises the tightly focused image of zero-energy electrons (see Sec. II E) provides an enhanced energy resolution. The suitability of this entrance lens design and the criteria for threshold detection has been discussed elsewhere.²² The spectrometer components and design will now be discussed in more detail.

A. Toroidal deflectors

The electron optical properties of toroidal deflectors have been studied by Toffoletto *et al.*,¹⁵ based upon earlier work by Wollnik,²³ resulting in general design formulae. Toroidal analyzers can be characterized in terms of a “cylindrical” radius, a (the distance from the interaction region to the toroidal deflector entrance), a “spherical” radius, b (the radius of the central path through the deflector), and a sector angle, θ , as defined in Fig. 2. Although toroidal analyzers have axial symmetry they are the topological link between the more familiar 127° cylindrical and hemispherical analyzers. Toffoletto *et al.*¹⁵ show that the focusing properties of toroids can be determined as a function of the sector angle, θ , and the “cylindrical-to-spherical radius ratio” ($c = a/b$) as shown in Figs. 2 and 3. They describe the focusing in the energy-dispersive, or radial, planes as “point-to-point” fo-

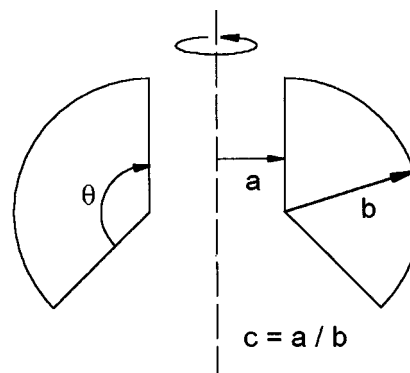


FIG. 2. A diagram showing the parameters that characterize toroidal surfaces, namely: cylindrical radius (a), spherical radius (b), and sector angle (θ).

cus. By introducing entrance and exit slits one constrains these positions to be image “points” in any radial plane. Under these conditions the point-to-point imaging conditions lie on a curve between cylindrical ($c = \infty$, $\theta = 127^\circ$) and hemispherical analyzers ($c = 0$, $\theta = 180^\circ$), as shown in Fig. 3.

Parallel trajectories from a small extended source in the axial plane, which is orthogonal to all the radial planes, are brought to a focus after deflecting through an angle ϕ in a toroidal analyzer. The angular focusing in the axial plane is termed “parallel-to-point” focusing and this condition can also be recognized in hemispherical analyzers. Parallel rays entering the hemisphere in the axial (or nonenergy dispersive) plane are brought to a focus after only 90° . The rays then diverge and leave the hemisphere after deflecting through 180° as parallel rays resulting in lateral image inversion. For angle-resolved studies, one requires the initial an-

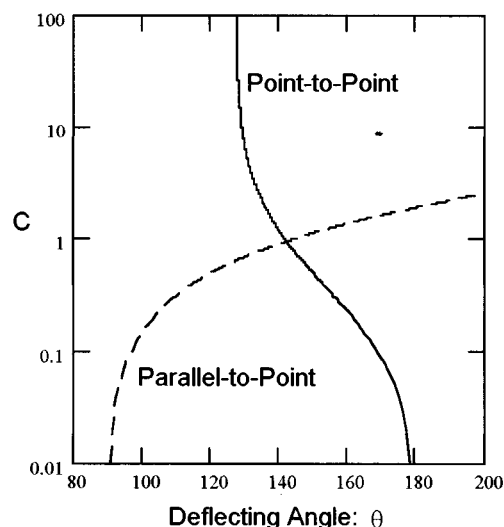


FIG. 3. A plot of the point-to-point (solid) and parallel-to-point (dashed) focusing conditions as a function of the toroidal parameters c and θ derived from the matrix formalism of Toffoletto *et al.* (Ref. 15). The point-to-point curve has asymptotic limits of 127° and 180° with the object and image positions at the entrance and exit surfaces of the toroids, respectively. In the case of parallel-to-point focusing, the object position is on the axis of symmetry due to the very weak focusing effects of the entrance lens in the axial plane.

gular information in the axial plane to be preserved, while maintaining the focusing conditions in the energy-dispersive plane. Therefore the variable, c , needs to be chosen so that $\phi = \theta$, i.e., the sector angle for point-to-point focusing also satisfies the condition for parallel-to-point focusing (see Fig. 3).

The decision as to the actual physical size of the analyzers was made after considering three main factors. The first was the aberration effects of a finite size interaction region on the toroidal focusing properties. In our perpendicular plane geometry, the size of the interaction region in the axial plane is determined by the diameter of the photon beam ($\sim 1-2$ mm, depending on choice of capillary) and in the radial plane by the electron optical properties of the entrance lenses (but is typically ~ 1 mm). As this size is essentially fixed, this can only be regarded effectively as a point source if it is small in comparison to the cylindrical radius, a . Second, the cylindrical radius determines the overall space for the entrance lens (which transports the electrons from the interaction region to the toroidal entrance slit) and for reasons that will be discussed in Sec. II C, this length should not be too small. Finally, the energy resolving power depends on the spherical radius, b , for a given entrance/exit slit width [see Eq. (2)]. After considering the accelerating and focusing capability of the entrance lens, and the overall range of electron energies one may want to transport with it ($\sim 1-50$ eV), a reasonable, minimum mean energy of the electrons transmitted through the toroidal analyzer can be ascertained (~ 5 eV). As the system should at least be capable of resolving diatomic vibrational levels, an appropriate value for the spherical radius, b , can be chosen.

Our design has a cylindrical radius of 95 mm and a spherical radius of 100 mm, giving $c = 0.95$ and a sector angle of 142° . This corresponds to axial focusing from the interaction region to the exit surfaces of the toroids, whereas the object in the radial plane is moved to the toroidal entrance slit by means of the entrance lens. The analysis of Toffoletto *et al.*¹⁵ does not take into account the acceleration effects of entrance and exit lenses on the toroidal focusing conditions; however, they have inserted similar lenses in their system and have “found no detrimental effects on the angular resolution.” Our analyzer system was then modeled using the SIMION (version 4.0) electron/ion lens package²⁴ which provided supporting evidence that the system—including the lenses—can be made to focus simultaneously in both the radial and axial planes.

The theoretical potentials on the inner and outer toroidal surfaces can be determined using the following expression:

$$V(r) = V_0 \left[1 + \left(2 + \frac{4}{c\pi} \right) \ln \left(\frac{2br + \pi ab}{2br + \pi ar} \right) \right], \quad (1)$$

where V_0 is the electron “pass” energy (eV_0) and r is the spherical radius of the toroidal surface.¹⁵ The expression for energy resolution [full width at half-maximum (FWHM)] can be expressed as

$$\frac{\Delta E_{\text{FWHM}}}{eV_0} = \frac{\omega}{Db} + \kappa \alpha^2, \quad (2)$$

where α is the maximum entrance half angle (in the energy dispersive plane), b is the spherical radius, ω is the width of the toroidal entrance and exit slits (assumed equal), and the dispersion $D = (c\pi + 2)/(c\pi + 1)$. Read *et al.*²⁵ have shown that κ for hemispherical analyzers ($D = 2$) is 0.25 and we have taken κ to be 0.33 for cylindrical analyzers ($D = 1$). For our system $D = 1.25$, $\omega = 1$ mm, $b = 100$ mm, $\alpha = 5^\circ$, and κ is assumed to be 0.3, resulting in a theoretical energy resolving capability of $\Delta E_{\text{FWHM}}/eV_0 = 1/100$, which models well what we achieve in practice.

The inner and outer toroids were made from aluminum alloy (Dural) due to its ease of machining, density, and availability; with a tolerance of ± 0.1 mm in every plane. The crucially important mechanical alignment was attained using several ball bearings with the same diameter as the intertoroidal gap (50 mm). All aluminum surfaces were coated with aerosol graphite to avoid field perturbations produced by surface oxidation and to reduce secondary electron emission. The toroids are partial and hence end effects produce electric field distortions which ultimately limit the useful angular range and alter the focusing properties of the analyzers, as they do in the lenses. In hemispherical analyzers (for example) it is common to insert corrective “hoops” in the end plane of the hemispheres to terminate the electric field; their potentials are adjusted semiempirically to optimize the energy resolution. Two similar corrective strips have been placed on both sides of the toroid entrance and exit slits. As the analyzers lack cylindrical symmetry, further strips etched on a printed circuit board are used to terminate the field at the edge planes of the partial toroids and so maximize the useful angular range.

B. Interaction region

The interaction region is defined by the intersection of the photon beam and of gas emanating from a copper hypodermic needle positioned orthogonal to the photon beam. Photons enter the interaction region via a Pyrex capillary tube, with an internal diameter of either 1 or 2 mm. The glass tube is supported within an aluminum pipe, with an endpiece which also contains an insulated cylinder which defines the photon beam divergence as shown in Fig. 4. This collimating cylinder is suitably biased to ensure none of its photoelectrons leave the endpiece, whose geometry is also designed to prevent the electric field from penetrating into the target vicinity. The interaction region is surrounded by a 40 mm diam cylindrical molybdenum foil (coaxial with the photon beam) which screens the photon beam path from the electric fields emanating from the toroid entrance lenses. During initial tests the target shield contained an array of holes, which allowed the photoelectrons to enter the analyzer lens system. The array of 2 mm diam holes, whose centers in the axial plane were spaced at 10° intervals as viewed from the interaction region, allowed the angular properties of the analyzers to be investigated. We now perform experiments using a continuous 6.5 mm wide annular slit instead of the array of holes. Two thin strips bridge the annular slit near the edges of the analyzer angular acceptance ranges. These serve as angle markers; their shadows are evident in the detected images as illustrated later in Fig. 8.

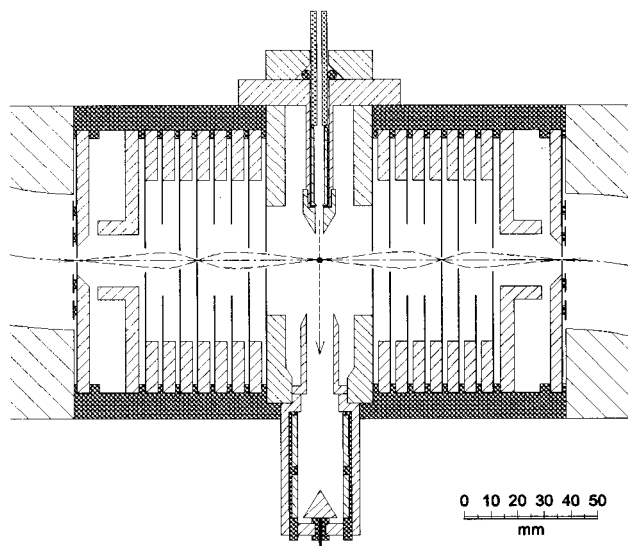


FIG. 4. A scale diagram showing the entrance lenses and target region in the spectrometer in the radial or energy-dispersive plane. In the diagram, the photon beam enters the interaction region from above, via a capillary, and its flux is monitored with an aluminum photodiode. The entrance lenses are the slits formed by a series of coaxial cylindrical surfaces of increasing radii. The acceptance angle in the radial plane is $\pm 6^\circ$ and the slit width variation among the lens elements is also shown.

An aluminum photodiode is used as a beam dump and flux monitor for the photons. The photodiode entrance is carefully designed to accommodate the divergent photon beam and to ensure no photoelectrons or electric fields penetrate back into the interaction region. The photodiode current is measured by an electrometer, whose analogue voltage output is converted to pulses using a voltage-to-frequency converter. These pulses are accumulated to provide a measure of the integrated photon flux.

C. Entrance lens

The lens elements on the two independent analyzers are slits on the curved surfaces of a series of coaxial cylinders, with increasing diameters, as shown in Fig. 4. The cylinders are made from nonmagnetic stainless steel and support molybdenum foil which constitutes the curved surface close to the electron beam. The cylinders are mounted on a rigid polyvinylidene fluoride disk to provide mutual insulation and mechanical alignment. The lens system contains seven elements (and a deflector) which behave like two multielement lenses providing an intermediate crossover in the vicinity of the central electrode.

When using an electron energy analyzer to detect low-energy photoelectrons the main concern is to avoid detecting background electrons of the same energy and/or trajectories which will take them through the analyzer exit slit. The main source of these undesirable electrons is a photoionization process from the target gas, with a large cross section and a lower threshold energy, resulting in high energy electrons emitted in all directions from the interaction region. These fast electrons will inevitably hit metal surfaces and liberate low energy electrons, some of which will be in the field of view of the analyzer. The intermediate crossover at the 2 mm

wide slit in the middle of the entrance lens is important as it restricts severely the image parameters, so reducing the quantity of background electrons from reaching the detector.

As a design starting position, the “curved-slit” entrance lens for this system was assumed to be described by the Harting and Read planar slit geometry.²⁶ As long as the slit width, h , is small compared to the radius of curvature of the element, r , the lens element can effectively be regarded as planar—to first order. Leckey²⁷ shows that this approximation is reasonable as long as $h/2r \ll 1$. This approximation (which only breaks down close to the interaction region) explains how one can achieve focusing in the radial plane, with only small effects in the axial plane. Once designed, the lens performance was then refined using SIMION. However, this was of limited use for studying the axial plane focusing as the then available version of SIMION assumed full axial symmetry, which is clearly inappropriate for our partial toroidal analyzers. Consequently, the resulting end effects of the lenses and analyzer could not be modeled effectively. In practice a printed circuit board (PCB) was used to terminate the lenses, which not only limits field penetration (from/to the neighboring lenses of the other analyzer) but avoids the charging effects of a simple insulating plate. The PCB incorporated additional “pads” where the interelement gap was relatively large, and whose potential could be altered empirically to provide the optimum lens termination. This additional complexity has proved most effective allowing the trajectories within 10° from the nominal angular limits to be focused at the detector. Nevertheless, due to noticeable image deformations at the edges, about a 20° loss in the angular range at each edge was adopted (and anticipated), reducing the useful analyzer angular acceptances to 60° and 140° in the axial plane. (Additional mechanical constraints limit its angular range in the 100° toroid to 60° anyway as the detector must be off-axis to allow the photon beam to pass by.)

Ideally there should only be focusing in the radial plane and none in the axial plane, but one effect of the lack of 360° symmetry in the lenses is to make them weakly focus in the axial plane. The degree of axial focusing depends on the quality of field termination at the lens edges and the potential differences between adjacent elements—particularly those close to the interaction region where the curvature is relatively large. Care was therefore exercised not to distort the angular scale by avoiding high potentials ($> \sim 80$ V) on those specific lens elements.

D. Exit lens

The exit lens, shown in Fig. 5 and which also contains a deflector close to the toroidal exit slit, transports the electrons from the toroid exit to the detection plane. The elements are formed from slits in the curved surfaces on a series of coaxial cones. Again, a simple planar slit was the starting point in the design and the final system was modeled on SIMION. This planar slit approximation is expected to be poorer for this “conical” lens system because the radii of the two curved edges on each element are different. This results in different trajectories above and below the optic axis. Significant aberrations were therefore expected in the image quality of this lens. To counter these effects, the lens was

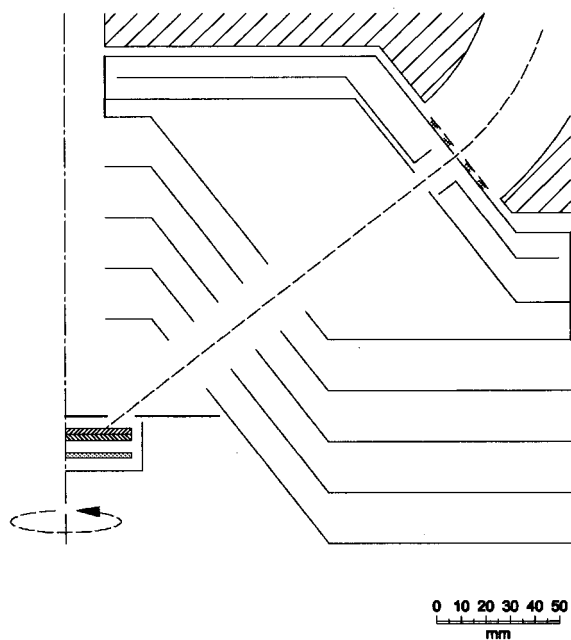


FIG. 5. A scale diagram of the exit lens which transports the angle-dispersed energy-resolved electrons from the exit of the toroidal analyzer to the two-dimensional position-sensitive detector. The elements are formed from slits in the curved surfaces on a series of coaxial cones and the electron beam impinges on the first of two microchannel plates at an angle of 52° to the normal.

designed to have a magnification of 0.5, giving a smaller image size on the detector. A simple four-element lens was designed, which is essentially a standard three-element lens with a movable central position for optimizing performance. These elements were made in 1 mm thick aluminum, using spinning techniques, and coated with aerosol graphite.

In principle, the electron image at the exit of the toroid is dispersed *radially* in energy and thus toroidal analyzers should give both energy *and* angle dispersed images. For a typical spectrometer one could envisage an energy-dispersed range of $\sim 10\%$ of the mean pass energy. Significantly, the success of this potentially powerful multidetection technique depends on the performance of the exit lens. This requires a conical lens system that can transport radially extended images with minimal aberrations so that at the detector one would obtain concentric circular images with different radii corresponding to different energies. We have not yet pursued this interesting option, but we are aware of others who are developing such lens systems.²⁸

E. Electron detectors and processing electronics

The two position-sensitive detectors (PSD) are each comprised of two microchannel plates (MCP), with a 40 mm diam active area, and two-dimensional resistive anode encoders supplied by Quantar Technology Inc. (model QT3394). The resistive anode is designed so that the charge cloud from the MCPs will be divided in linear proportion among the four corners, depending on the relative position of incidence. The corners of the anode are capacitively coupled to shaping preamplifiers, which lie just outside the vacuum system and are connected to the QT2401A "position com-

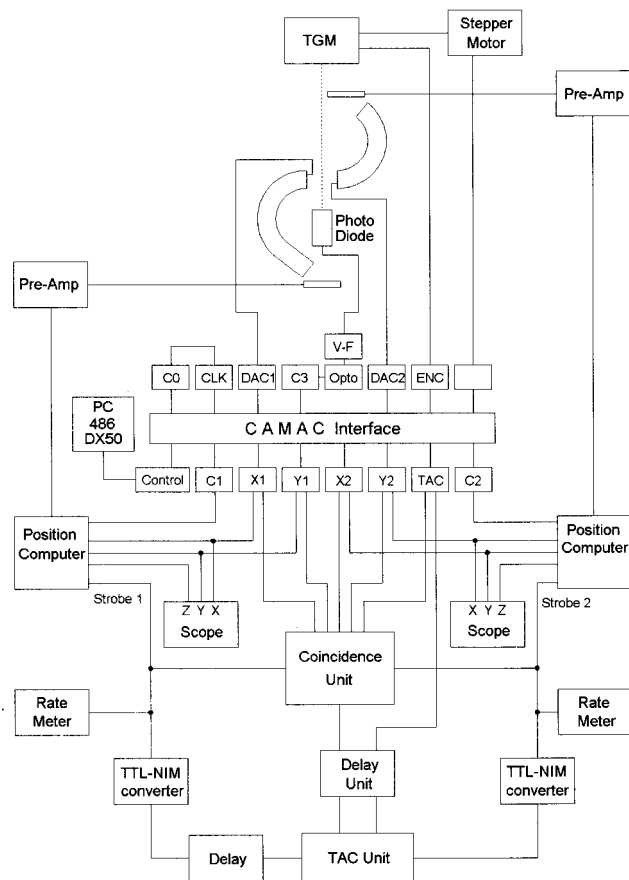


FIG. 6. A diagram showing the processing electronics and computer interfacing. Most items are self-explanatory and are discussed in the text. C_n = counters, ENC = grating encoder unit, CLK = clock pulse, $V-F$ + Opto = floating electrometer, voltage-to-frequency converter, and optoisolator photon flux monitoring system.

puter." It computes the position of incidence using analogue ratio methods and provides 0.5–4.5 V (x, y) output pulses. Two 20 MHz oscilloscopes display the (x, y) information from the position computer, so providing a "live" image of the detector which is invaluable for tuning and monitoring the spectrometer.

The spectrometer is controlled by a dedicated 486DX66 PC via a CAMAC interface. CAMAC has been adopted for the hardware link as the apparatus functions at the Daresbury SRS which has standardized on this system. A schematic diagram of the processing electronics is shown in Fig. 6. Parallel output registers are used to address external 12-bit digital-to-analog converters, allowing the detected electron energies to be scanned. The movement of the toroidal grating monochromator is controlled using a CAMAC stepper motor unit and the photon energy is monitored. A dual counting module (Borer 1008) is used as a clock pulse counter and also accumulates the photon flux (see Sec. II B).

For noncoincident spectra, the information from both detectors can be recorded independently. If one is only interested in integrated count rates [i.e., the (x, y) information is ignored], TTL "strobe" pulses from both detectors are input to CAMAC counters (Kinetic Systems 3640). (An additional useful feature of the position computer is its image gating

system, which allows one to restrict the area on the detector's image from which one accumulates counts, thereby enabling angle-resolved experiments to be performed.) The CAMAC counting modules are configured so that an accurate value of the data accumulation time can be evaluated. The (gated) (x,y) image from a detector can also be recorded using CAMAC 12-bit ADC modules (Borer 1245) which digitize the analogue pulses from the position computer. These ADC modules have 12-bit resolution and also contain a 256 word buffer to help reduce dead time.

For coincidence experiments, timing pulses from the two analyzers must also be processed, in addition to the (x,y) positional information. The timing pulses are obtained from the two TTL strobe pulses by using their fast rising edges to trigger a TTL-to-NIM converter (LeCroy 222). These pulses are fed into a time-to-amplitude converter (TAC) (Tennelec TC862) as in conventional coincidence experiments. If there is a valid TAC output then there will always be positional information from the two PSDs available for this event. The positional information from the two resistive encoders is gated with the TAC unit, so removing the majority of uncorrelated events. The TAC signal is also delayed as the processing of the timing signals is quicker than that of the (x,y) information from the resistive encoders. Thus, the coincidence unit synchronizes the two modes of data processing and is used to instigate the analog-to-digital conversion of the TAC output and the corresponding two (x,y) values. The (five) ADC modules obviously operate asynchronously to the computer system, which empties and stores the data once their buffers are full. They start their conversions with appropriate TTL pulses derived from the strobe pulses, whose purpose is to indicate the presence of "valid" analog (x,y) pulses.

The count rate limitation in the electronics is governed ultimately by that of the charge division method in the position computer, and is typical of such resistive anode encoders. The detector is effectively a spatially extended "single" detector as it can only process one event over its active area at any one time. For image-integrated (TTL) counting purposes, the count rate limitation is < 100 kHz. For measurements requiring (x,y) image detection, the 12-bit ADC conversion requires $13 \mu\text{s}$ and further time jitter (particularly between the two detectors in coincidence mode) restricts the (x,y) imaging count rate to < 50 kHz. Additionally, CAMAC interrupt handling and the asynchronous nature of the data collection currently restricts further our (x,y) image data collection to count rates of < 10 kHz. These different dead-time limitations could be improved significantly by purpose-built hardware. These count rate restrictions are just tolerable for single photoionization studies as one can generally reduce the count rate by improving the electron and/or photon resolutions—which is usually desirable anyway. For coincidence counting where the count rates are $\sim 1 \text{ s}^{-1}$, no such dead-time constraints exist.

III. RESULTS

Examples of the angle-dispersed images produced by the toroidal analyzers are shown in Fig. 7. The well-defined images are clearly circular arcs and have therefore suffered

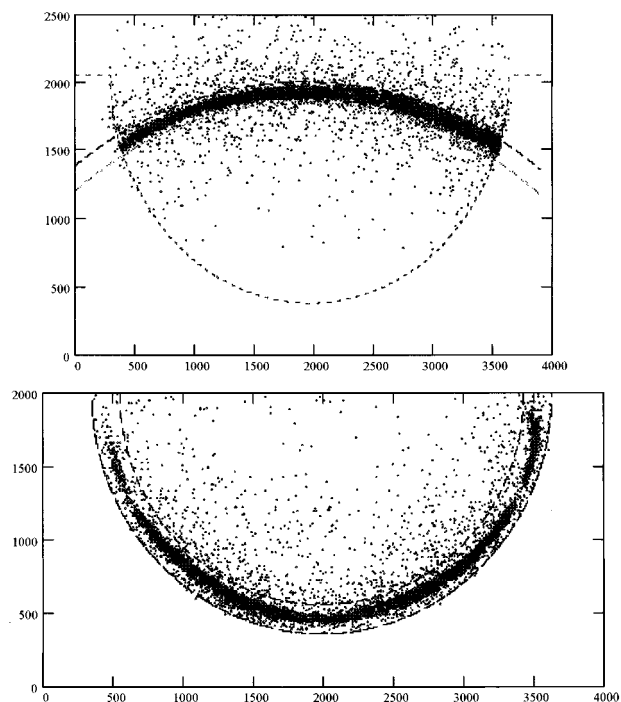


FIG. 7. Angle-dispersed and energy-resolved photoelectron images from the 180° and 60° analyzers. The lack of intensity in the vicinity of 20° and 160° degrees in the large analyzer's image is due to the angle markers which are used to check the angular scale, as discussed in Secs. II B and III. The dashed radii on either side of the sharp images indicate the radial ranges used in further analysis, as discussed in the text.

little distortion from the electron optics. These (x,y) images are first converted to polar (r,θ) format and radially filtered to use only the electrons within an annular ring centered on the sharp image in further analysis.

In angle-dispersed images, the linearity of the angular scale and its extent needs to be checked as they can be altered significantly by the careless use of either the entrance or exit lens. Physical "stops" marking the extremities of the image at 20° and 160° in the 180° analyzer are clearly identifiable in the recorded image (see also Fig. 8). The position of the physical stops in the recorded image can indicate that the angular scale is slightly demagnified, particularly for low photoelectron energies (< 0.5 eV), requiring a small linear stretch—from the center outwards—to restore it to the laboratory scale.

Furthermore, each part of the annular image can be thought of as independent as the electron trajectories responsible for that part are unique. Therefore variations in the yield as a function of θ will occur because of local electric field irregularities, mechanical differences (e.g., entrance and exit slit sizes), microchannel plate gain variations, and the inevitable edge effects. The resulting (angular) differential nonlinearity is remarkably stable for a particular spectrometer tuning and so a normalization function can easily be found. Just as measured energy scales in photoelectron spectra need to be calibrated with a feature of known energy, so angular distributions have to be relative to a reliable standard. In the case of single photoionization, the angular distribution for the He^+ , $n=1$ state is the yardstick as it has an asymmetry parameter $[\beta(E)]$ of 2 for all photoelectron energies

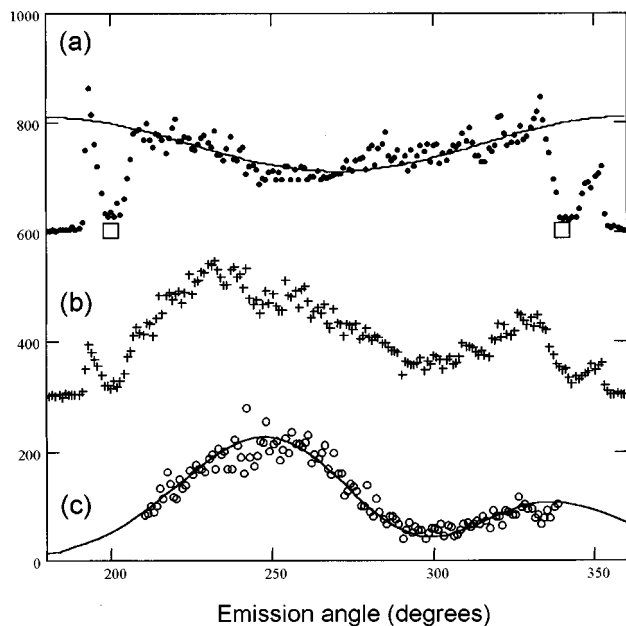


FIG. 8. (a) The angular distribution of the He^+ ($n=2$) level at 10 eV above threshold measured with the large (180°) analyzer (points) and the calculated distribution for the same process for $P=0.83$ and $\beta=0.57$ (full line). The positions of the angle markers are indicated by large squares at 200° and 340° . (b) A distribution of 10 eV electrons recorded by the large analyzer in coincidence with an electron of the same energy detected anywhere on the small analyzer, for the same orientation of the spectrometer as for (a) and after the subtraction of random counts. (c) Measurement (b) corrected for the angular efficiency variation derived from (a) (open circles), compared with the calculated sum of the TDCS (full line) as discussed in Sec. III. All the measured spectra have been radially filtered and are presented in 1° intervals.

(i.e., $\cos^2 \theta$ distribution). The He^+ , $n=2$ level can also be used as its asymmetry parameter is reasonably well known as a function of energy²⁹ and acts as an important consistency check, particularly at low photoelectron energies where its β is nearly 0 (isotropic distribution). These measurements are made regularly throughout the data collection process and are used both to determine the degree of polarization of the light source and to derive the angular normalization curve. An example of the normalization procedure is illustrated in Fig. 8.

A typical distribution of coincident events—or TAC spectrum—is shown in Fig. 9. As the toroidal analyzers and their acceptance angles are large, the inherent transit time spread in the electron trajectories dominates the width of the coincidence peak, rather than the simple but effective way of deriving fast timing pulses described in Sec. II E. The distribution of random events is uniform and we have found no need for a noise antenna to remove electrical pickup.^{30,31}

For each coincident event the TAC output, Δt , and the (x, y) coordinates from both detectors are digitized and stored. In the subsequent analysis, radial filtering is applied to remove the electrons outside the sharp image (see Fig. 7) and time filtering is used to subtract “random” events from under the coincidence peak. Optimizing the statistical requirements for the latter procedure has been discussed by McCarthy and Weigold.³² By integrating over 10° intervals (say) on both images a two-dimensional matrix

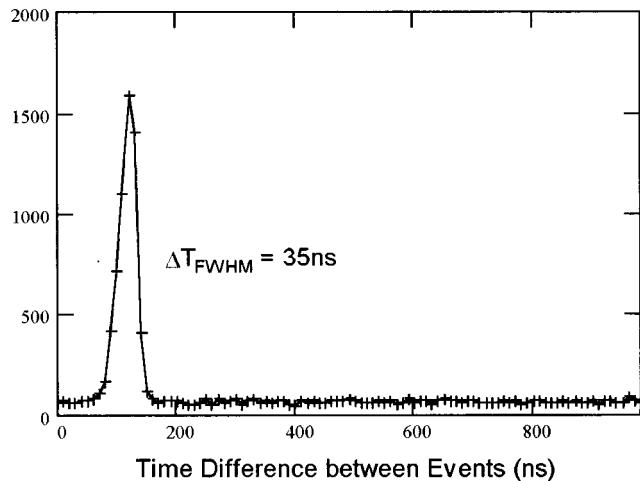


FIG. 9. A spectrum of the time distribution of coincident events for 10 + 10 eV electrons in helium, integrated over the acceptance angles of both analyzers. The true-to-random ratio varies with photoelectron energy and spectrometer orientation (with respect to the polarized light source). Typical values in helium vary between 5–50 with “true” coincidence count rates of 0.1 – 1.0 s^{-1} .

($^{180}\theta_j, ^{60}\theta_k$) containing the angular distributions of the “true” coincidences is created. The coincidence matrix is then multiplied by a correction matrix derived from the angular normalization functions of both analyzers, as described earlier. This procedure assumes that the two analyzers are imaging identical areas in the interaction region so that the coincidence volume is the same for all matrix elements. This cannot be guaranteed experimentally, but with careful handling of the lens potentials—especially minimizing the use of deflectors—the results show it is a reasonable approximation in practice. Such coincidence volume problems are inherent in this kind of experiment and are well recognized in conventional spectrometers.

Angular distributions for the electrons emitted in the photodouble ionization of helium normalized in this way are displayed in Fig. 10. These distributions are obtained from the coincident data used in Fig. 8 and show the dramatic variation of the TDCS both with θ_1 and θ_{12} , the mutual

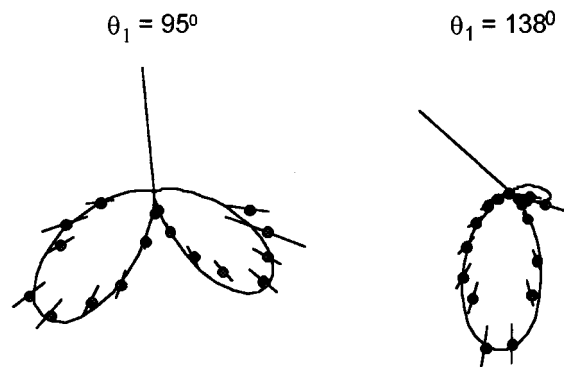


FIG. 10. The polar plot of two triple differential cross sections for 10 + 10 eV electrons in helium with the angle between one ejected electron (a 10° section centered on θ_1) and the light polarization direction (horizontal) as indicated. The TDCSs are arbitrarily normalized to the theory of Huetz *et al.* (Ref. 11) (solid curve) as discussed in the text, having taken into account the degree of linear polarization ($S_1=0.83$).

angle between the two electrons. The TDCS were measured at the equal energy sharing condition of 10+10 eV and are compared with theoretical distributions using the formalism of Huetz *et al.*,¹¹ with a Gaussian correlation function having a half angle of 88° ($\pm 3^\circ$). Similar distributions have also been obtained for 5+5 eV and 20+20 eV conditions.³³ The essential feature of these distributions is the persistent presence of a node at a mutual emission angle of 180°. The two electrons leave the ion in opposite hemispheres, as one might expect from electron correlation, but the node arises at equal energy sharing conditions due to symmetry restrictions associated with the $^1S^e \rightarrow ^1P^0$ transition.¹¹ The general agreement with the theoretical curves is excellent; further studies will focus on the fine details of the electron correlation function.

ACKNOWLEDGMENTS

The authors gratefully acknowledge the financial support for the project from EPSRC and a CASE award with VSW Scientific Instruments Ltd. for G.R., along with University studentships for G.W.B. and J.P.W. Credit is also due to Express Engineering, who manufactured the toroidal deflectors, and to Quantar Technology Inc. for their postsales support with regard to the detectors. The authors wish to acknowledge the contributions to this project of many individuals and organizations. To all the members of the Departmental Mechanical and Electronics workshops, especially Alan Bott, Ken Patterson, Peter Harrison, Peter Lang, Chris Burrow, and Jeff Reah.

The authors would like to thank members of Newcastle's Atomic and Molecular Physics Group for their support, in particular Dr. Barry Peart for the loan of a helium discharge lamp for initial tests. We acknowledge the valuable assistance of Dr. Mike MacDonald while performing the experiments at Daresbury. T.J.R. would also like to thank Professor John Mitchell at Newcastle, and colleagues at Manchester University—notably Drs. John Comer, Anthony Wills, and Peter Hammond—for their helpful discussions and encouragement.

¹O. Schwarzkopf, B. Krässig, J. Elmiger, and V. Schmidt, Phys. Rev. Lett. **70**, 3008 (1993).

²P. Lablanquie, J. Mazeau, L. Andric, P. Selles, and A. Huetz, Phys. Rev. Lett. **74**, 2192 (1995).

³P. Lablanquie, J. H. D. Eland, I. Nenner, P. Morin, J. Delwiche, and M. J. Hubin-Franskin, Phys. Rev. Lett. **58**, 992 (1987).

- ⁴G. Dujardin, S. Winkoun, and S. Leach, Phys. Rev. A **31**, 3027 (1985).
- ⁵R. I. Hall, G. Dawber, A. McConkey, M. A. MacDonald, and G. C. King, Phys. Rev. Lett. **68**, 2751 (1992).
- ⁶R. Dörner, J. M. Feagin, C. L. Cocke, H. Bräuning, O. Jagutzki, M. Jung, E. P. Kanter, H. Khemliche, S. Kravis, M. H. Prior, H. Schmidt-Böcking, L. Spielberger, J. Ullrich, M. Unversagt, and T. Vogt, Phys. Rev. Lett. **77**, 1024 (1996).
- ⁷A. Huetz, P. Lablanquie, L. Andric, P. Selles, and J. Mazeau, J. Phys. B **27**, L13 (1994).
- ⁸O. Schwarzkopf, B. Krässig, V. Schmidt, F. Maulbetsch, and J. S. Briggs, J. Phys. B **27**, L347 (1994).
- ⁹G. Dawber, L. Avaldi, A. G. McConkey, H. Rojas, M. A. MacDonald, and G. C. King, J. Phys. B **28**, L271 (1995).
- ¹⁰O. Schwarzkopf and V. Schmidt, J. Phys. B **28**, 2847 (1995); **29**, 1877 (1996).
- ¹¹A. Huetz, P. Selles, D. Waymel, and J. Mazeau, J. Phys. B **24**, 1917 (1991).
- ¹²F. Maulbetsch and J. S. Briggs, J. Phys. B **26**, 1679 (1993).
- ¹³A. K. Kazansky and V. N. Ostrovsky, Phys. Rev. A **51**, 3712 (1995).
- ¹⁴M. Pont, R. Shakeshaft, F. Maulbetsch, and J. S. Briggs, Phys. Rev. A **53**, 3671 (1996).
- ¹⁵F. Toffoletto, R. C. G. Leckey, and J. D. Riley, Nucl. Instrum. Methods Phys. Res. B **12**, 282 (1985).
- ¹⁶H. A. Engelhardt, A. Zartner, and D. Menzel, Rev. Sci. Instrum. **52**, 1161 (1981).
- ¹⁷R. G. Smeenk, R. M. Tromp, H. H. Kersten, A. J. H. Boerboom, and F. W. Saris, Nucl. Instrum. Methods **195**, 581 (1982).
- ¹⁸R. C. G. Leckey and J. D. Riley, Appl. Surf. Sci. **22/23**, 196 (1985).
- ¹⁹D. T. Young, A. G. Ghielmetti, E. G. Shelley, J. A. Marshall, J. L. Burch, and T. L. Bokker, Rev. Sci. Instrum. **58**, 501 (1987).
- ²⁰J. H. Flexman, J. F. Williams, and P. A. Hayes, J. Phys. IV **3C6**, 79 (1993).
- ²¹S. Cvejanović and F. H. Read, J. Phys. B **7**, 1841 (1974).
- ²²S. Cvejanović, G. W. Bagley, and T. J. Reddish, J. Phys. B **28**, 3571 (1994).
- ²³H. Wollnik, *Focusing of Charged Particles*, edited by A. Septier (Academic, New York, 1967), Vol. 2, pp. 164–202.
- ²⁴D. A. Dahl, J. E. Delmore, and A. D. Appelhans, Rev. Sci. Instrum. **61**, 607 (1990).
- ²⁵F. H. Read, J. Comer, R. E. Imhof, J. N. H. Brunt, and E. Harting, J. Electron Spectrosc. Relat. Phenom. **4**, 293 (1974).
- ²⁶E. Harting and F. H. Read, *Electrostatic Lenses* (Elsevier, Amsterdam, 1976).
- ²⁷R. C. G. Leckey, J. Electron Spectrosc. Relat. Phenom. **43**, 183 (1987).
- ²⁸Y. Kato, H. Tanuma, N. Kobayashi, W. Wu, Y. Yamazaki, A. Danjo, and M. Yoshino (private communication).
- ²⁹R. Wehlitz, B. Langer, N. Berrah, S. B. Whitfield, J. Viehhaus, and U. Becker, J. Phys. B **26**, L783 (1993).
- ³⁰P. Hayes, M. A. Bennett, J. Flexman, and J. F. Williams, Rev. Sci. Instrum. **59**, 2445 (1988).
- ³¹J. Lower and E. Weigold, J. Phys. E **22**, 421 (1989).
- ³²I. E. McCarthy and E. Weigold, Phys. Rep. **27**, 275 (1976).
- ³³T. J. Reddish, J. P. Wightman, S. Cvejanović, Proceedings of the 18th Symposium of the Physics of Ionised Gases Kotor, Yugoslavia, 1996 (to be published).